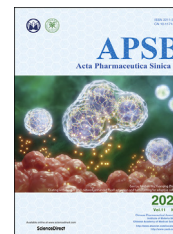




Chinese Pharmaceutical Association  
Institute of Materia Medica, Chinese Academy of Medical Sciences

Acta Pharmaceutica Sinica B

[www.elsevier.com/locate/apsb](http://www.elsevier.com/locate/apsb)  
[www.sciencedirect.com](http://www.sciencedirect.com)



ORIGINAL ARTICLE

# Coating with flexible DNA network enhanced T-cell activation and tumor killing for adoptive cell therapy



Ziyan Zhang<sup>a,c,†</sup>, Qiaojuan Liu<sup>b,†</sup>, Jizhou Tan<sup>d,†</sup>, Xiaoxia Zhan<sup>d</sup>,  
Ting Liu<sup>d</sup>, Yuting Wang<sup>b</sup>, Gen Lu<sup>e,\*</sup>, Minhao Wu<sup>b,\*</sup>,  
Yuanqing Zhang<sup>a,c,\*</sup>

<sup>a</sup>School of Pharmaceutical Sciences, Sun Yat-sen University, Guangzhou 510006, China

<sup>b</sup>Zhongshan School of Medicine, Sun Yat-sen University, Guangzhou 510080, China

<sup>c</sup>National and Local United Engineering Lab of Druggability and New Drugs Evaluation, Sun Yat-sen University, Guangzhou 510006, China

<sup>d</sup>The First Affiliated Hospital, Sun Yat-sen University, Guangzhou 510080, China

<sup>e</sup>Guangzhou Institute of Pediatrics, Guangzhou Women and Children's Medical Centre, Guangzhou Medical University, Guangzhou 510080, China

Received 22 January 2021; received in revised form 11 March 2021; accepted 28 March 2021

## KEY WORDS

Cell surface engineering;  
Selective cytoprotection;  
DNA nanostructure;  
Tetrahedral DNA  
nanostructure;  
Rolling circle amplification;  
Adoptive cell therapy;  
T cell;  
Tumor-killing

**Abstract** Adoptive cell therapy (ACT) is an emerging powerful cancer immunotherapy, which includes a complex process of genetic modification, stimulation and expansion. During these *in vitro* or *ex vivo* manipulation, sensitive cells are inescapably subjected to harmful external stimuli. Although a variety of cytoprotection strategies have been developed, their application on ACT remains challenging. Herein, a DNA network is constructed on cell surface by rolling circle amplification (RCA), and T cell-targeted trivalent tetrahedral DNA nanostructure is used as a rigid scaffold to achieve high-efficient and selective coating for T cells. The cytoprotective DNA network on T-cell surface makes them aggregate over time to form cell clusters, which exhibit more resistance to external stimuli and enhanced activities in human peripheral blood mononuclear cells and liver cancer organoid killing model. Overall, this work provides a novel strategy for *in vitro* T cell-selective protection, which has a great potential for application in ACT.

© 2021 Chinese Pharmaceutical Association and Institute of Materia Medica, Chinese Academy of Medical Sciences. Production and hosting by Elsevier B.V. This is an open access article under the CC BY-NC-ND license (<http://creativecommons.org/licenses/by-nc-nd/4.0/>).

\*Corresponding authors.

E-mail addresses: [lugen5663330@sina.com](mailto:lugen5663330@sina.com) (Gen Lu), [wuminhao@mail.sysu.edu.cn](mailto:wuminhao@mail.sysu.edu.cn) (Minhao Wu), [zhangyq65@mail.sysu.edu.cn](mailto:zhangyq65@mail.sysu.edu.cn) (Yuanqing Zhang).

†These authors made equal contributions to this work.

Peer review under responsibility of Chinese Pharmaceutical Association and Institute of Materia Medica, Chinese Academy of Medical Sciences.

<https://doi.org/10.1016/j.apsb.2021.04.002>

2211-3835 © 2021 Chinese Pharmaceutical Association and Institute of Materia Medica, Chinese Academy of Medical Sciences. Production and hosting by Elsevier B.V. This is an open access article under the CC BY-NC-ND license (<http://creativecommons.org/licenses/by-nc-nd/4.0/>).

## 1. Introduction

In past decades, adoptive T cell therapy (ACT), which is also called T-cell transfer therapy, has shown significant progress in cancer immunotherapy<sup>1,2</sup>. Several types of transferred T cells have been applied in preclinical or clinical trials of ACT, including tumor-infiltrating lymphocytes (TIL), genetically modified T cells like chimeric antigen receptor (CAR)-T or T cell receptor (TCR)-T cells<sup>3</sup>. In these ACT, T cells are collected from patients or healthy donors, followed with *in vitro* expansion and/or genetic modification, and then infused back to the patient<sup>3,4</sup>. Unlike immortalized cell line, primary T lymphocytes are very sensitive to unfavorable external stimuli. However, the manufacture process of generating T cells *in vitro* often takes 2–8 weeks in the lab. Multiple steps such as pipetting, washing, centrifugation, as well as unfavorable culture conditions like nonoptimal pH, osmotic pressure or media<sup>5–9</sup>, may lead to cell damage or even death<sup>10,11</sup>.

Although researchers have been trying hard to promote cell resistance to unfavorable culture conditions or harmful external stimuli (e.g., physical forces, UV exposure, toxic compounds)<sup>5–9,12–14</sup> during manufacture process<sup>15,16</sup>, the effect is still not good. Several cell surface engineering strategies for cell protection have been developed<sup>11,17</sup>, including electrostatic deposition of polyelectrolytes<sup>9,12–14,18,19</sup>, biomineralization<sup>5,6</sup>, as well as metal ion complexation<sup>7,8,20</sup>. However, challenges still remain, largely limiting their biomedical application. For example, the deposited monomers or degraded polymers or metal ion complexation have varying degrees of toxicity<sup>21–23</sup>, thus may decrease cell viability and proliferation. Biomineralization often forms a tight and hard shell<sup>5</sup>, which may compromise the interaction of cell surface receptors and their ligands<sup>12,18,20,24–26</sup>, thereby suppressing T cell activation and killing efficiency.

Recently, naturally synthesized biopolymers like DNA have attracted increasing attentions in biomedical engineering fields, due to their good biocompatibility and tunable properties. DNA-based materials display many advantages in living cell encapsulation<sup>9,27</sup>, for their excellent performance on biosafety, stability, accessibility, as well as precise programmability and functionalization<sup>28,29</sup>. Rolling circle amplification (RCA) is a commonly used isothermal enzymatic amplification method that can easily produce bulk DNA materials<sup>30,31</sup>. The RCA products are also a kind of high-molecular-weight polymer which can naturally intertwine with each other, forming a DNA porous network<sup>32,33</sup>. Tetrahedral DNA nanostructure (TDN) can be prepared simply by self-assembling oligonucleotides, with a defined valence, rigid and stable structure<sup>34–36</sup>. After functionalization with cholesterol or nucleic acid aptamer, TDN can firmly anchor on the cell membrane for further applications<sup>37–41</sup>.

To be noted, so far, T-cell isolation is still the prerequisite step for current T-cell protection strategy, due to lack of selective coating, and therefore some sensitive and fragile cells may be damaged during the process of T-cell separation. In this regard, to enhance the T-cell viability and activity in ACT, an efficient T cell-specific cytoprotective method is highly required, which can selectively protect T cells from unfavorable stimuli before, rather than after, the step of T-cell separation.

In the present study, we developed a high-efficient and one-step selective cytoprotection strategy for T cells. Using T cell-targeted trivalent TDNs as scaffolds, we successfully performed

the RCA reaction on the T-cell membrane with a high selectivity, by which T cells can be coated with a flexible DNA network before isolation. The cytoprotective DNA network made T cells aggregate over time to form cell clusters, which displayed more resistance to external stimuli. Moreover, this selective protection strategy also enhanced T-cell activity and tumor-killing efficiency in human peripheral blood mononuclear cells (PBMCs) and primary liver cancer organoid killing model. Overall, the present study provides a powerful method to protect T cell *in vitro*, and therefore shows a great potential in biomedical application of adoptive T-cell therapy.

## 2. Materials and methods

### 2.1. Ethics statement

This study and all experiment protocols were approved by the Clinical Research and Experimental Animal Ethics Committee of the First Affiliated Hospital of Sun Yat-Sen University (2018 [43]). For experiments with human samples, informed consent was obtained from all participants.

### 2.2. Materials and reagents

All DNA oligonucleotides used in this work were synthesized by Sangon Biotech Co., Ltd. (Shanghai, China). Their sequences are listed in Supporting Information Table S1. 1 × TE Buffer, 10 × TM Buffer, 10 × TBE Premixed Powder and DNA Marker were purchased from Sangon Biotech Co., Ltd. (Shanghai, China). T4 DNA Ligase, phi29 DNA Polymerase and Deoxynucleotide (dNTP) Solution Mix were purchased from New England Biolabs Inc. (Ipswich, MA, USA). YeaRed Nucleic Acid Gel Stain, 6 × Loading Buffer, cell membrane dye DiO, Calcein-AM and Cell Counting Kit-8 (CCK-8) were purchased from Yeasen Biotech Co., Ltd. (Shanghai, China). 7-Amino-4-chloromethylcoumarin (CMAC) was purchased from KeyGEN BioTECH Co., Ltd. (Nanjing, China). Phosphate-Buffered Saline (PBS, Gibco), Roswell Park Memorial Institute (RPMI) 1640 cell culture medium (Gibco), Dulbecco's modified Eagle's medium (DMEM) cell culture medium (Gibco), fetal bovine serum (FBS, Gibco), penicillin–streptomycin (Gibco), CellTrace Far Red (Invitrogen) and caspase 3/7 fluorescent apoptosis probe (Invitrogen) were purchased from Thermo Fisher Scientific Inc. (Waltham, MA, USA). Hexamethyldisilazane (HMDS), collagenase IV, DNase and Y-27632 were purchased from Sigma–Aldrich. Hydrogen peroxide solution 30% (w/w) were purchased from Aladin. Reduced growth factor BME2 was purchased from R&D Systems Inc. (Minneapolis, MN, USA). MycoAlert Mycoplasma Detection Kit and X-Vivo 15 Lymphocyte Medium were purchased from Lonza (Basel, Switzerland). IL-2 is purchased from PerproTech (Cranbury, NJ, USA). TrypLE Express is purchased from STEMCELL Technologies Inc. (Vancouver, Canada).

### 2.3. Cell culture

Jurkat cells were cultured in RPMI 1640 medium supplemented with 10% FBS and 1% penicillin–streptomycin. MCF-7 cells were cultured in DMEM medium supplemented with 10% FBS and 1% penicillin–streptomycin. All cells were cultured at 37 °C with 5% CO<sub>2</sub> in a cell incubator.

#### 2.4. Self-assembly of TDN and RCA reaction performed in buffer

All DNA oligonucleotides were dissolved and were diluted to 100  $\mu\text{mol/L}$  in  $1 \times \text{TE Buffer}$  (10 mmol/L Tris-HCl, 1 mmol/L EDTA, pH 8.0), obtaining stock solution. To synthesize the tetrahedral DNA nanostructure (TDN), DNA oligonucleotides were mixed together equimolarly firstly and diluted to desired concentration (according to experimental designs) with  $10 \times \text{TM buffer}$  (the final components were 50 mmol/L Tris-HCl, 8 mmol/L  $\text{MgSO}_4$ , pH 7.5). Next, the mixture was heated at 95  $^\circ\text{C}$  for 10 min, then quickly cooled to 4  $^\circ\text{C}$  and maintained at 4  $^\circ\text{C}$  for at least 10 min in a Thermal Cycler (Bio-rad T100, Hercules, CA, USA). Finally, the synthesized TDNs solution was stored at 4  $^\circ\text{C}$  before use. To perform the rolling circle amplification (RCA) reaction in buffer, the TDNc-RCA-primer (5  $\mu\text{L}$ , 10  $\mu\text{mol/L}$ ) and RCA template (5  $\mu\text{L}$ , 10  $\mu\text{mol/L}$ ) were mixed together and incubated at 37  $^\circ\text{C}$  for 30 min. Then,  $10 \times \text{T4 DNA Ligase Reaction buffer}$  (1.5  $\mu\text{L}$ ), T4 DNA Ligase (0.5  $\mu\text{L}$ , 400 cohesive end units/ $\mu\text{L}$ ) and Milli-Q water (3  $\mu\text{L}$ ) were added and incubated at room temperature for 2 h to form circular RCA template. Finally,  $10 \times \text{phi29 DNA Polymerase Reaction Buffer}$  (2  $\mu\text{L}$ ), phi29 DNA Polymerase (1  $\mu\text{L}$ , 10 U/ $\mu\text{L}$ ) and dNTP Solution Mix (2  $\mu\text{L}$ , 10 mmol/L each) were added, followed by a 1-h reaction at 37  $^\circ\text{C}$ , forming a gel-like product.

#### 2.5. Constructing flexible DNA network-coated cell (DNC-Cell) or DNC-Cell cluster by cell surface engineering

Firstly, TDNa-Linker, TDNb-Linker, TDNc-RCA-primer, TDNd-Linker (1  $\mu\text{L}$ , 100  $\mu\text{mol/L}$  each) and LD201t1-Linker (3  $\mu\text{L}$ , 100  $\mu\text{mol/L}$ ) were mixed together, followed by diluted with  $10 \times \text{TM buffer}$  (1  $\mu\text{L}$ ). The final concentration was 12.5  $\mu\text{mol/L}$ . Then, the mixture was heated at 95  $^\circ\text{C}$  for 10 min, then quickly cooled to 4  $^\circ\text{C}$  and maintained at 4  $^\circ\text{C}$  for at least 10 min, to form the T cell-targeted trivalent TDNs. Next, RCA template (5  $\mu\text{L}$ , 12.5  $\mu\text{mol/L}$ ) hybridizing with TDNc-RCA-primer were added to the prepared T cell-targeted trivalent TDNs (5  $\mu\text{L}$ , 12.5  $\mu\text{mol/L}$ ), followed by a 30-min incubation at 37  $^\circ\text{C}$ . Then,  $10 \times \text{T4 DNA Ligase Reaction Buffer}$  (1.5  $\mu\text{L}$ ), T4 DNA Ligase (1  $\mu\text{L}$ , 400 cohesive end units/ $\mu\text{L}$ ) and  $10 \times \text{TM buffer}$  (2.5  $\mu\text{L}$ ) were added and then incubated at room temperature for 2 h to form circular TDN-RCA-templates. Subsequently,  $5 \times 10^5$  cells were washed with PBS, then suspended in an RCA reaction buffer (200  $\mu\text{L}$ ): Tris-HCl (50 mmol/L),  $\text{MgCl}_2$  (10 mmol/L),  $(\text{NH}_4)_2\text{SO}_4$  (10 mmol/L), DTT (4 mmol/L), the prepared TDN-RCA-templates, and dNTPs (0.2 mmol/L) in  $1 \times \text{serum-free RPMI 1640 medium}$ . After pulsing a phi29 DNA Polymerase (2  $\mu\text{L}$ , 10 U/ $\mu\text{L}$ ), the RCA reaction was performed at 37  $^\circ\text{C}$  for different time according to experimental designs.

#### 2.6. Verifying the formation process of the TDN and the RCA reaction via agarose gel electrophoresis

3% Agarose gel was prepared in  $1 \times \text{TBE buffer}$  (89 mmol/L Tris-boric, 2 mmol/L EDTA, pH 8.0) and then stained with YeaRed Nucleic Acid Gel Stain. Each DNA sample (8.5  $\mu\text{L}$ , 2.5  $\mu\text{mol/L}$ ) was mixed with a  $6 \times \text{loading buffer}$  (1.5  $\mu\text{L}$ ), and ran at 100 V for 60 min in  $1 \times \text{TBE}$  with an ice-water bath. A 25–500 bp DNA marker was used as a reference molecular weight standard. For verifying the RCA reaction, 4% agarose gel was used.

#### 2.7. Confocal laser scanning microscopy (CLSM) imaging

Cy3-labeled short oligonucleotides (Cy3-C-strand) complementary to partial DNA network was used as a fluorescent indicator of the RCA production (the DNA network) on the cell membrane. They were added to the cell suspension 10 min after the reaction began at a final concentration of 1  $\mu\text{mol/L}$ . When the reaction ended, cells were washed with PBS twice and then stained with cell membrane dye DiO at room temperature for 15 min. After washed with PBS twice, cells were resuspended in PBS and imaged by CLSM (Olympus, FV3000, Tokyo, Japan).

#### 2.8. Scanning electron microscopy (SEM) imaging

Cells were washed with PBS twice then fixed by glutaraldehyde (500  $\mu\text{L}$ , 2.5%) overnight at 4  $^\circ\text{C}$ . Fixed cells were washed with PBS twice, and gradient dehydrated with a series of ethanol solutions (30%, 50%, 70%, 90%, 95%, and 100%) for 15 min each step. Subsequently, cells were resuspended in 100% hexamethyldisilazane (HMDS), following by dropping onto clean silicon wafers and dried by air in a fume cupboard overnight. After spraying with gold, cell samples were imaged by Field Emission SEM (Quanta 250 FEG, FEI, Hillsboro, OR, USA) at an accelerating voltage of 20 kV.

#### 2.9. Transmission electron microscopy (TEM) imaging

Cells were fixed with glutaraldehyde and  $\text{OsO}_4$ , and then gradient dehydrated with ethanol and acetone. The fixed samples were embedded in resin and cut by using an ultramicrotome to obtain thin sections. The thin sections were stained with uranyl acetate and lead citrate, followed by imaged via TEM (FEI, Tecnai G2 Spirit Twin, Hillsboro, OR, USA).

#### 2.10. Comparison among TDN anchored on cells, Apt-RCA and TDN-RCA occurred on cells via CLSM imaging and flow cytometry

The equimolar TDNc-C-strand, LD201t1-RCA-primer and TDNc-RCA-primer were used in this experiment. The TDNc-C-strand' was incubated with cells at 37  $^\circ\text{C}$  for 30 min. The RCA reaction using single strand LD201t1 aptamer (Apt-RCA) or that using trivalent TDN scaffold (TDN-RCA) was performed at 37  $^\circ\text{C}$  for 30 min. Cy3-C-strands were added to the cell suspension 10 min after the reaction began, at a final concentration of 1  $\mu\text{mol/L}$ . After washed with PBS twice, cells were resuspended in PBS for following assays. In flow cytometer (Beckman Coulter, Inc., CytoFLEX S, Brea, CA, USA) assay,  $1 \times 10^4$  events were recorded for each sample.

#### 2.11. Fluorescent inverted microscopy

The RCA reactions proceeded for 0.5, 1, 1.5, 2 or 2.5 h, respectively, forming DNC-Cell clusters in different sizes. The fluorescent indicator Cy3-C-strands were also used to show the DNA network between cells. Cells were washed with PBS twice immediately, followed by resuspending in PBS. Cells were seeded on a 12-well plate then imaged by Fluorescent Inverted Microscope (IX83, Olympus, Tokyo, Japan). The DNC-Cell clusters were measured and counted by cellSens software version 1.16, (Olympus, Tokyo, Japan), using a measurement function. The size means the average diameter of the clusters and was fitted by Gaussian fitting using GraphPad Prism 7, software (San Diego,

CA, USA). The percentage of DNC–Cell clusters is calculated by the number of cells that formed clusters dividing the number of total cells.

### 2.12. Cell proliferation assay

$5 \times 10^4$  cells/mL cells were seeded on a 35 mm culture dish. The cells were cultured in RPMI 1640 medium supplemented with 10% FBS and 1% penicillin–streptomycin at 37 °C with 5% CO<sub>2</sub> in a cell incubator. After culture for 24, 48 or 72 h, the cells were harvested and tested *via* CCK-8. The optical density (OD) at 450 nm was measured using a microplate reader (BMG LAB-TECH, FLUOstar Omega-ACU, Ortenberg, Germany).

### 2.13. Verifying the selective coating of T cell

Jurkat cells were pre-stained with Calcein-AM at 37 °C for 15 min. MCF-7 cells were pre-stained with CMAC at 37 °C for 25 min. The prestained Jurkat cells and MCF-7 cells were mixed together in a ratio of 1:3. Then, the RCA reaction was performed in the mixed cell suspension for 30 min. After washed with PBS twice, cells were resuspended in PBS and imaged by fluorescent inverted microscope (Olympus). For testing the selective coating of T cells in human PBMCs, human PBMCs isolated from healthy donors were firstly treated with RCA reaction for 30 min and then stained with FITC-anti human CD3 antibody (Biolegend #317306), followed by CLSM imaging or flow cytometry analysis, respectively.

### 2.14. Examining cells tolerating external stimuli via cell viability assays

Cells were pretreated with or without RCA reaction, rinsed and suspended in PBS, and then tested for tolerance to following external stimuli. The DNC–Cell groups were treated with RCA reaction for 30 min. The DNC–Cell clusters groups were treated with RCA reaction for 1 h, (1) UV exposure: cells ( $5 \times 10^5$  cells/mL) were seeded on a UV transparent 96-well plate and were placed in a darkroom equipped with a UV-C Lamp (PHILIPS, TUV8W G8T5, Holland). The distance between the plate and the lamp was 5 cm. After exposure to UV for 0, 15, 30, 60, 90 or 120 min in room temperature, respectively, the cell viability was tested *via* CCK-8. (2) Relative centrifugal force: 200  $\mu$ L cells ( $1 \times 10^5$  cells) were added to a 1.5 mL centrifuge tube and were centrifuged for 30 min, at the relative centrifugal force of 0,  $1 \times 10^3$ ,  $5 \times 10^3$ ,  $10 \times 10^3$ ,  $15 \times 10^3$  or  $20 \times 10^3 \times g$ , respectively. After that, the cell viability was tested *via* CCK-8. (3) pH: cells ( $1 \times 10^5$  cells) were rinsed with NaCl (153.8 mmol/L) and suspended in NaCl (10  $\mu$ L, 153.8 mmol/L). 10  $\mu$ L cell suspension was added to 190  $\mu$ L solution with the same ion strength and the final pH was 5, 6, 7.4, 8 or 9 respectively. After incubation for 2 h in room temperature, the cell viability was tested *via* CCK-8. (4) Osmotic pressure: 10  $\mu$ L cell suspension ( $1 \times 10^5$  cells) was added to 190  $\mu$ L 0.1  $\times$  PBS, 0.25  $\times$  PBS, 0.5  $\times$  PBS, 0.75  $\times$  PBS, 1  $\times$  PBS, 2  $\times$  PBS, 3  $\times$  PBS, 4  $\times$  PBS or 5  $\times$  PBS respectively. After incubation for 2 h in room temperature, the cell viability was tested *via* CCK-8. (5) Reactive oxygen species (ROS): 10  $\mu$ L cell suspension ( $1 \times 10^5$  cells) was added to 190  $\mu$ L H<sub>2</sub>O<sub>2</sub> solution. The H<sub>2</sub>O<sub>2</sub> concentration was 0, 0.5, 1, 2, 4, 6 or 8 mmol/L in PBS respectively. After incubation for 1 h in room temperature, the cell viability was tested *via* CCK-8.

### 2.15. Isolation of PBMCs and flow cytometry analysis

PBMCs were isolated from fresh blood of healthy donors by Ficoll–Hypaque centrifugation. Then, PBMCs were resuspended with RCA reaction buffer for indicated time points (0.5, 1 or 2 h), while control group were treated with RCA buffer without phi29 DNA Polymerase for 2 h. After RCA reaction, PBMCs were washed with PBS twice and then collected immediately as inactivated PBMCs. For activation group, PBMCs were pretreated with agonistic anti-CD3/CD28 Abs (1  $\mu$ g/mL) for 24 h before collection. Then inactivated or activated PBMCs were stained in PBS with the following Abs, including Zombie NIR™ Fixable Viability Kit (Biolegend #423105), PerCP/Cyanine5.5 anti-human CD3 (Biolegend #317336), PE anti-human CD69 (Biolegend #310906), APC anti-human IL-2 (Biolegend #500310), PE/Cy7 anti-human IFN- $\gamma$  (Biolegend #502528), and then detected on a flow cytometer (BD Biosciences, BD FACSVerser, San Jose, CA, USA) and analysed with FlowJo software (Becton, Dickinson and Company, Ashland, OR, USA).

### 2.16. Ex vivo culture and expansion of tumor organoids and autologous tumor infiltrating lymphocytes (TILs)

Human primary liver cancer-derived organoid culture and autologous TIL *ex vivo* expansion was performed as previously described by our group and others<sup>42,43</sup>. Human tissue and specimens were obtained by surgical resection from patients of primary liver cancer and segregated into average two parts. One part was used for organoid culture, and another was used for TIL expansion. For organoid culture, tumor surgical resections were mechanically disintegrated into small pieces (0.5–1 mm<sup>3</sup>) and incubated with the digestion solution, which contained 2.0 mg/mL collagenase IV, 0.1 mg/mL DNase and 10 mmol/L Y-27632 for 30 min. Then the digested cell suspension was filtered through 100 mm nylon net, centrifuged, and seeded in the reduced growth factor BME2 (basement membrane extract, Type 2) with the cell density at 5000–10,000/100  $\mu$ L per well in a 24-well plate. Incubate the plate at 37 °C for 20 min until the BME2 was solidified. Added 100  $\mu$ L per well organoid expansion medium as described before. Organoids were passaged approximately every week and harvested before using (within 5 passages). All organoids were regularly checked for mycoplasma contamination using the MycoAlert Mycoplasma Detection Kit.

For autologous TIL *ex vivo* expansion, tumor samples were cut into small pieces in X-Vivo 15 Lymphocyte Medium. IL-2 at 6000 IU/mL was used for expansion. All cells were cultured at 37 °C with 5% CO<sub>2</sub> for 2 weeks. After expansion, TILs were collected and pretreated with RCA reaction buffer with or without phi29 DNA Polymerase for 1 h, and then used in the following experiments.

### 2.17. Organoids killing assay

After cell counting, organoids were resuspended in IL-2 free human HCC organoids medium and seeded in flat-bottom plate with RCA or control vehicle-pretreated autologous TILs at a 10:1 effector:target (*E:T*) ratio. Tumor organoids were resuspended in X-Vivo15 medium and seeded in triplicate of flat-bottom plate with  $1 \times 10^5$  autologous TILs pretreated with RCA reaction buffer with or without phi29 DNA Polymerase for 1 h. To facilitate visualization, T cells were previously stained with 1 mmol/L of CellTrace Far Red. A fluorescent apoptosis probe which can detected activated

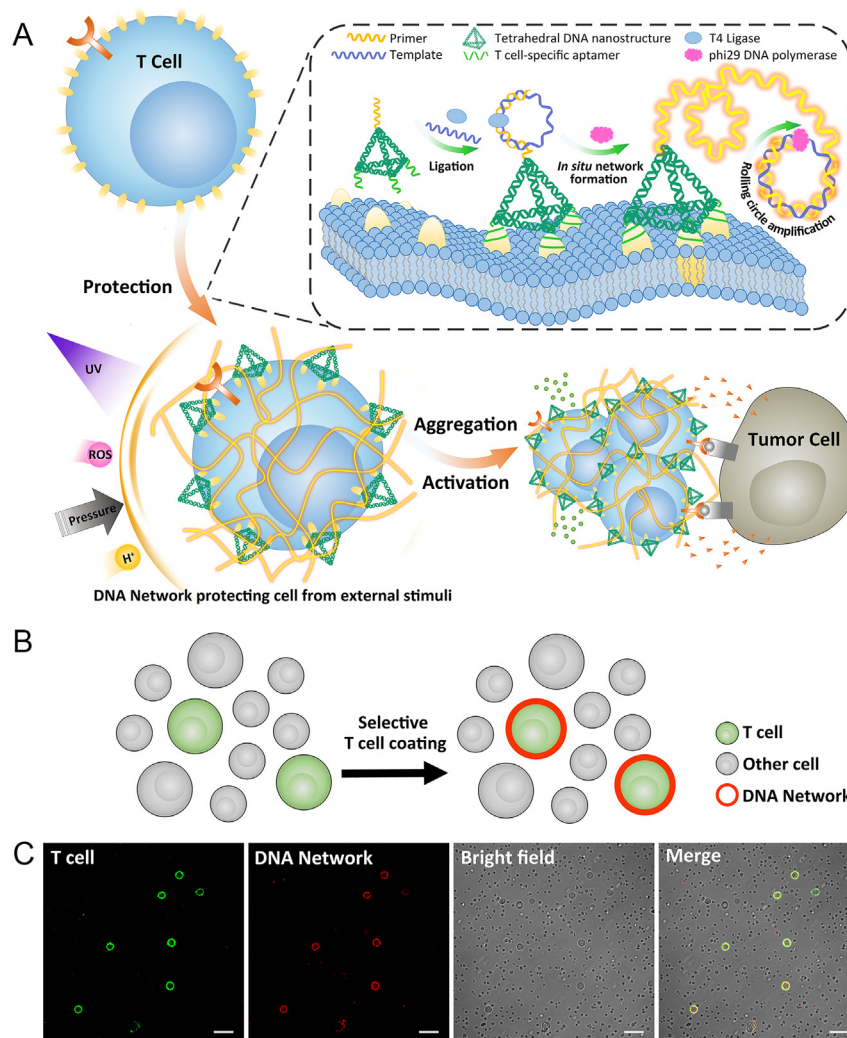


**Figure 1** T cell-selective coating and protection strategy with a flexible DNA network promotes T-cell aggregation and activation for anti-tumor therapy. (A) T cell selective protection strategy by constructing a flexible DNA network on T cell surface using *in situ* RCA reaction and a T cell-targeted trivalent TDN scaffold. (B) Schematic diagram of T cell-selective coating in heterogeneous cell populations. (C) The efficiency and specificity of our selective T-cell coating strategy was confirmed in human PBMCs by immunofluorescent confocal microscopy. Green: T cells stained with FITC-anti human CD3 antibody. Red: DNA network hybridized to short oligonucleotides labeled with Cy3. Scale bar: 20 μm.

caspace 3/7 (1:2000 dilution) was added at the beginning of co-culture to visualize cell apoptosis. After 24 h of co-culture, immunofluorescence microphotography images were taken using a Lionheart™ FX Automated Live Cell Imager (BioTek, Winooski, VT, USA) at indicated time points of killing (0, 8, 16, and 24 h).

For the quantification of the results, these images were further analyzed with Imaris software version 7.4 (Bitplane AG, Zurich, Switzerland), using the Spot function to locate and enumerate TILs and apoptotic cells inside the organoids, based on size and intensity threshold. The initial infiltration of T cells inside the organoids was considered as zero.

For flow cytometry, tumor organoids were cocultured with autologous TILs at a 10:1 E:T ratio for 6 h, and then dissociated into single cell with TrypLE Express. Cells were stained with Zombie NIR™ Fixable Viability Kit, PerCP/Cyanine5.5 anti-human CD3, PE anti-human CD69, APC anti-human IL-2, PE/Cy7 anti-human IFN-γ, and then detected on a flow cytometer (BD Biosciences) and analysed with FlowJo software (Becton, Dickinson and Compan).

### 2.18. Statistical analysis

The differences between two groups were analyzed using an unpaired two-tailed Student's *t*-test, while differences between  $\geq 3$  groups were compared by one-way analysis of variance (ANOVA), followed by Bonferroni post test. Data are considered statistically significant at  $P < 0.05$ .

## 3. Results and discussion

### 3.1. Graphical abstract: T cell-selective coating and protection strategy with a flexible DNA network promotes T-cell aggregation and activation for anti-tumor therapy

We constructed a flexible DNA network on T-cell surface by *in situ* RCA reaction and used trivalent TDN as a scaffold by virtue of its firm membrane adhesion ability. The trivalent TDN has an RCA primer at one vertex and three T cell-specific aptamer (LD201t1)<sup>44,45</sup> at the others. As shown in Fig. 1, five DNA

oligonucleotides self-assemble to form T cell-targeted TDN scaffolds. Next, the RCA templates bind to RCA primers and form circular RCA templates by T4 DNA ligase. TDN scaffolds specifically anchor onto the cell membrane. Then, RCA reaction occurs *in situ* on the cell membrane with the help of phi29 DNA polymerase. Many long single strand DNAs (ssDNAs) containing lots of repeating units complementary to the RCA template will form on the cell membrane. Finally, these long ssDNAs intertwine with each other and form a flexible DNA network on the cell membrane.

### 3.2. Successful construction of the T cell-targeted trivalent TDN scaffold

The TDN was made up of four oligonucleotides (TDNa, TDNb, TDNc and TDNd), each side of which has 17 base pairs (bp). To form the trivalent TDN scaffold, we designed a 20 nucleotides (nt) linker and added it to the 3' end of TDNa, TDNb, and TDNd (denote as TDNa-Linker, TDNb-Linker, and TDNd-Linker),

forming a free oligonucleotide linker at three vertexes of TDN respectively. Thus, three aptamers can precisely bind to three vertexes of TDN *via* hybridization.

First, we used 3% agarose gel electrophoresis to verify the step-by-step formation of T cell-targeted trivalent TDN scaffolds. As shown in Supporting Information Fig. S1A, from left to right, when sequentially adding relevant oligonucleotides, the main band increasingly moves slowly than the previous one due to a formed larger DNA nanostructure. These results confirmed the successful self-assembly of the T cell-targeted trivalent TDN scaffolds. Flow cytometry data showed that the T cell-targeted trivalent TDN scaffold can bind to Jurkat cell, an acute T cell leukemia cell line, while the TDN without aptamer cannot (Supporting Information Fig. S1B).

### 3.3. Selective coating with DNA network by *in situ* RCA reaction on T cell surface

To perform RCA reaction, we designed a TDNc-RCA-primer, which has an RCA primer at its 3' end. It is partly complementary

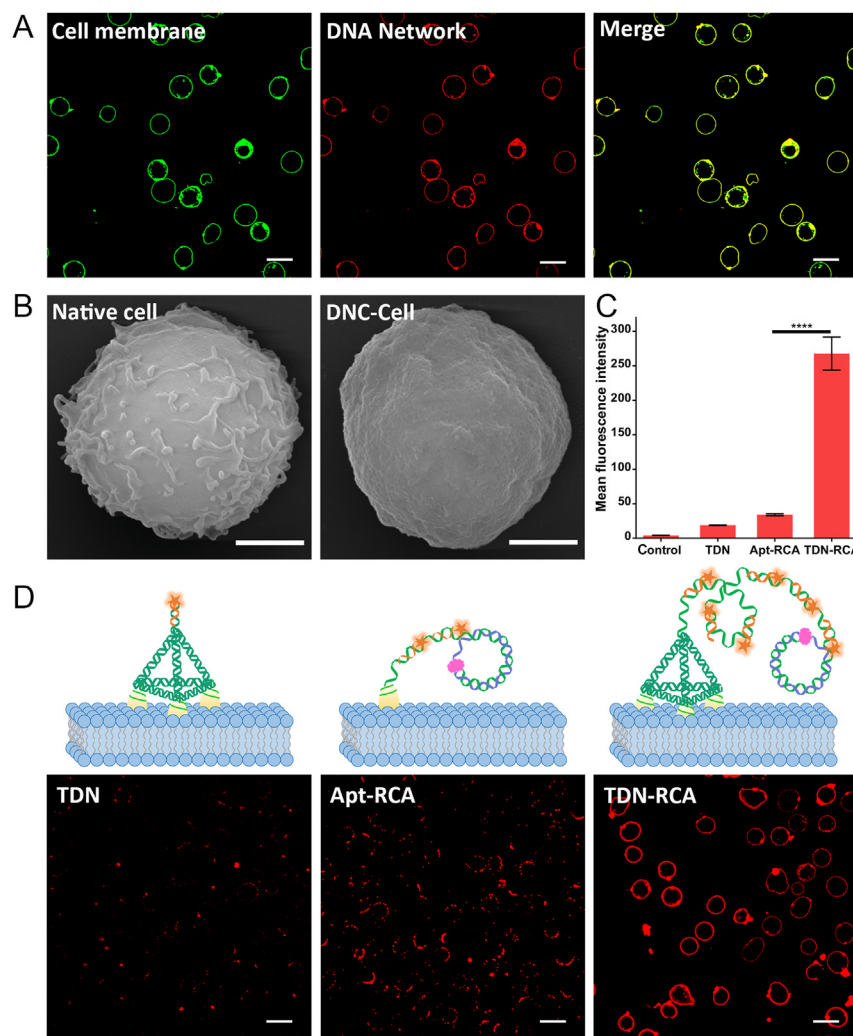


**Figure 2** Characterization of the DNC-Cell. (A) Confocal laser scanning microscope images of the flexible DNA network formed on Jurkat cell membrane. Green: cell membrane stained with DiO. Red: DNA network hybridized to short oligonucleotides labeled with Cy3. Scale bar: 20  $\mu\text{m}$ . (B) Scanning electron microscope images of native Jurkat cell, Jurkat cell coated with DNA network (DNC-Cell). Scale bar: 2  $\mu\text{m}$ . (C) The mean fluorescence intensity of Cy3-labeled TDN or DNA network on cell surface was detected by flow cytometry. Data are shown as mean  $\pm$  SD ( $n = 3$ ); \*\*\*\* $P < 0.0001$ . (D) Schematic diagrams and representative confocal laser scanning microscope images of the TDN, Apt-RCA, TDN-RCA treated cells. The red fluorescence indicates the TDN or DNA network on cell membrane. Scale bar: 20  $\mu\text{m}$ .

to the RCA template. Supporting Information Fig. S2 shows the 4% agarose gel electrophoresis image of each step in the RCA reaction. When T4 DNA ligase was added, a strong band with a size between 50 and 75 bp was detected, indicating the formation of circular RCA templates. When phi29 DNA polymerase was added, the band stayed at the inlet (lane 6), while only the circular RCA template's band was found without the addition of polymerase (lane 5), indicating the formation of high-molecular-weight RCA products.

We next performed the *in situ* RCA reaction on the cell surface. When the TDNc-RCA-primer self-assembled with other four oligonucleotides (TDNa-Linker, TDNb-Linker, TDNd-Linker and LD201t1-Linker), these RCA primers can firmly anchor to the cell membrane *via* trivalent TDN scaffolds.

We also designed a Cy3-labeled short oligonucleotide (Cy3-C-strand) as a fluorescent indicator, which is complementary to partial RCA products. If the RCA reaction occurred, products

containing continually replicated sequences will form. The Cy3-C-strand binds to the products and then a strong red fluorescence can be observed. The CLSM images (Fig. 2A) of the Jurkat cells after RCA reaction show colocalization of the cell membrane (green) and the DNA network (red), which indicates that the *in situ* RCA reaction successfully occurred on cell membrane, forming the DNA network-coated cells (DNC-Cells). The strong and dense red fluorescence of the DNA network indicates that the RCA products twining around each other on the cell membrane. The SEM images (Fig. 2B) show a shell-like morphology in the surface of the DNC-Cell compared with the native cell. The TEM images (Supporting Information Fig. S3) show a lot of dense filaments coating on the cell membrane of DNA-Cell, which are the long ssDNAs produced by RCA reaction, while the cell membrane without RCA treatment is very smooth. These results further confirmed a successful coating with the RCA products on the cell. The DNA network had little effect on cell activity, with a cell

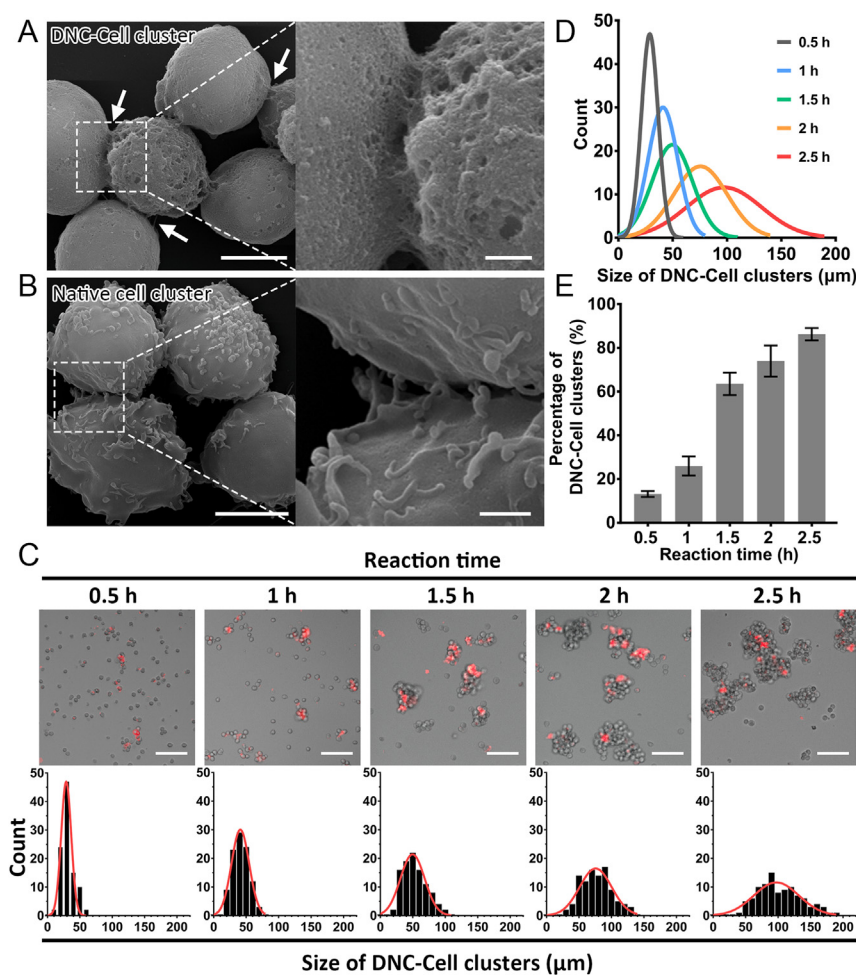


**Figure 3** Characterization of the DNC-Cell clusters formed by the DNA network intertwining with each other on the cell membrane. The DNC-Cell cluster was defined as three or more than three cells aggregated together. Scanning electron microscope images of (A) DNC-Cell cluster and (B) native cell cluster. Scale bar of the left is 5 μm and the right is 1 μm. The white arrows indicate the flexible DNA network gathering the DNC-Cells together. (C–E) Jurkat cells were treated with RCA reaction for indicated time points, and the formation of DNC-Cell clusters was examined by microscopy. (C) Above: representative images at indicated reaction time points. Red: the DNA network gathering cells together. Scale bar: 100 μm. Below: size statistical data at each time point. The size (D) and percentage (E) of DNC-Cell clusters were analyzed at indicated time points and statistical data are representative of three independent experiments. The curves show the Gaussian fitting of corresponding data. Each graph shows the random measurements of 100 clusters.

viability of  $97.8 \pm 1.1\%$  as tested by Cell Counting Kit-8 (CCK-8) (Supporting Information Fig. S4).

As the major cell type in current ACT, T cells are sensitive to external stimuli, however, to date, selective protection strategy for T cells remains lacking. To achieve T cell specific protection without pre-isolation, we used a T cell-targeted trivalent TDN scaffold which contains a T cell-specific aptamer, therefore ensure the selective coating with DNA network on T cell surface in one step. As shown in Supporting Information Fig. S5, MCF-7 cells (human breast cancer cell line) and Jurkat cells (human T cell line) were mixed together and then tested for the selectivity and efficiency of RCA reaction. After treatment, the red fluorescence of DNA network was observed around Jurkat, rather than MCF-7 cells, confirming the high selectivity of T cell coating in our strategy. Moreover, we further examined the effect of this T cell protection strategy in human PBMCs, which includes a variety of immune cells like T cells, B cells, nature killing cells, monocytes and etc. After treating with RCA reaction, PBMCs were stained with anti-CD3-FITC antibody, and then detected by immunofluorescent confocal microscopy and flow cytometry, respectively. As shown in a representative confocal image (Fig. 1C), in PBMCs, all the DNA network (Cy3 positive, red fluorescence) formed by RCA reaction was localized on T cell surface (CD3 positive, green fluorescence), whereas other cells in PBMCs were not coated. We further confirmed the selective coating efficiency in PBMCs isolated from three healthy donors using flow cytometry. As shown in Supporting Information Fig. S6, in all the three healthy donors, more than 98% of PBMCs were either Cy3 and CD3 double positive (T cells, coated with DNA-network) or negative (other cells, not coated with DNA network), indicating that our selective coating strategy for T cells was highly specific and efficient.

### 3.4. Trivalent TDN scaffold improved the efficiency of *in situ* RCA reaction

To further explore the role of the trivalent TDN scaffold on *in situ* RCA reaction, flow cytometry and CLSM were applied to compare the efficiency of RCA reaction on cell membrane between single strand LD201t1 aptamer (Apt-RCA) and trivalent TDN scaffold (TDN-RCA) group, using the fluorescent indicator (Cy3-C-strand) (Fig. 2C and D and Supporting Information Fig. S7). TDN group without RCA reaction only showed some weak spots around the cell. The TDN-RCA group showed strong and clear red fluorescence circle around the cells, while the Apt-RCA group shows some incomplete circles around the cells. The relative fluorescence intensity of the TDN-RCA was about 7.87-fold stronger than that of the Apt-RCA. These results indicated that RCA reaction can be much more efficient when using trivalent TDN as a primer scaffold. We attribute this to the firm membrane anchoring ability of trivalent TDN scaffold. It can anchor on the cell membrane with high binding affinity and maintain upright in the vertical direction, making it easy for the DNA polymerase to bind to the primer. While the single strand aptamer on cell membrane tend to sway and topple on the cell membrane, which reduces the chance for DNA polymerase to bind to the primer and slow down the RCA reaction.

### 3.5. DNA network-coated cells (DNC-Cells) aggregated over time to form cell clusters with different sizes

We found that the DNC-Cells aggregated over time and formed cell clusters. The representative SEM images show some connecting filaments (as indicated by white arrows in Fig. 3A)

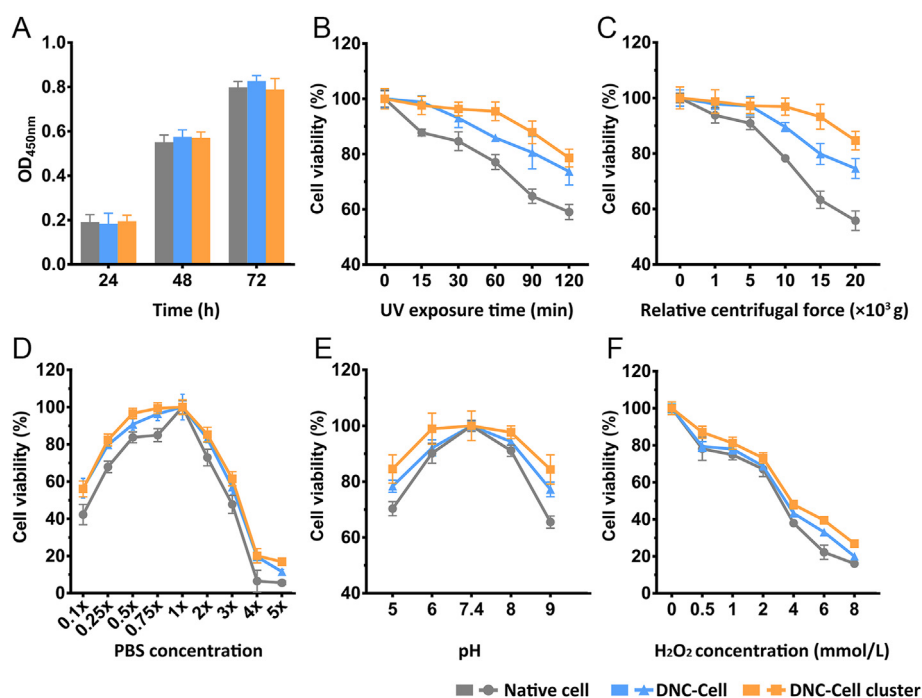


**Figure 4** DNC-Cells and DNC-Cell clusters displayed higher resistance to external stimuli than naive cell. (A) Cell proliferation (indicated by the optical density value at 450 nm) was comparable among native cells, DNC-Cells and DNC-Cell clusters within 72 h after reaction, as detected by CCK-8 assay. (B–F) Cell viability assay was performed in each group in response to different external stimuli: (B) UV exposure time, (C) relative centrifugal force, (D) PBS concentration, (E) pH and (F) H<sub>2</sub>O<sub>2</sub> concentration. The cell viability of DNC-Cells and DNC-Cell clusters was much higher than that in native cells, upon external stimulations.

between adjacent DNC–Cells, rather than native cells (Fig. 3B), suggesting that the DNA network formed by RCA reaction promotes DNC–Cell aggregation. The representative images (Fig. 3C, above) and the size statistical data (Fig. 3C, below) of DNC–Cell clusters at indicated time points are shown. Each graph shows the random measurement of 100 clusters. The red fluorescence between the cells in the clusters indicates the formed DNA network, which further demonstrates that it was the DNA network that gathered the cells together. The size of DNC–Cell clusters increased from about 30 to 100  $\mu\text{m}$  within 2.5 h after the RCA reaction started (Fig. 3D). Meanwhile, the percentage of DNC–Cell clusters also increased over reaction time, from about 13.1% to 86.2% (Fig. 3E).

Next, CCK-8 assay was applied to evaluate the effect of DNA network on cell proliferation. After incubation for 24, 48 or 72 h in a cell incubator, both DNC–Cells and DNC–Cell clusters showed comparable optical density (OD) at 450 nm, similar to that in native cells (Fig. 4A), indicating that the DNA network did not affect cell proliferation.

### 3.6. DNC–Cell clusters displayed higher resistance to external stimuli than DNC–Cells

Next, the cell viability of DNC–Cell clusters, DNC–Cells or native cells were detected in response to distinct stimuli, including UV exposure, relative centrifugal force, osmotic pressure, pH and

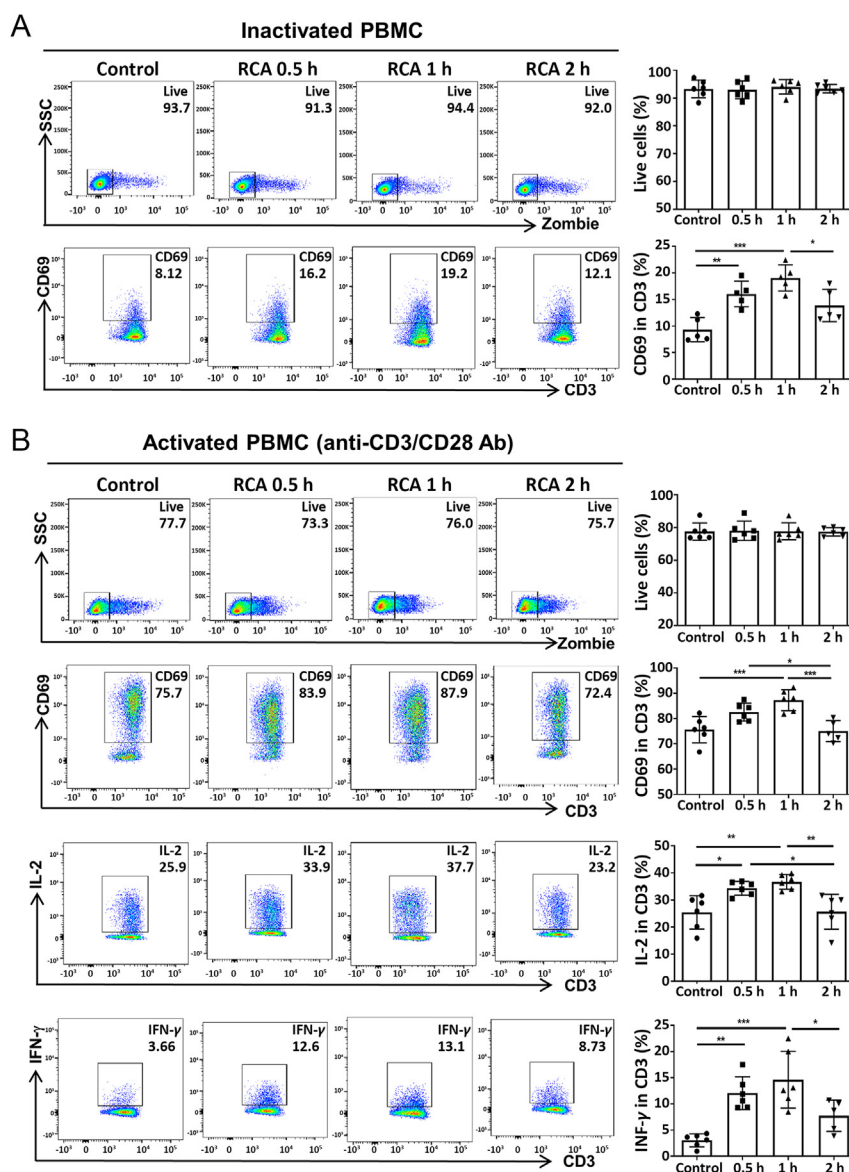


**Figure 5** Coating with DNA network promoted T-cell activation in human PBMCs without affecting the cell viability. Human PBMCs isolated from healthy donors ( $n = 6$ ) were treated with RCA reactions at indicated time points, and then detected for cell viability and T-cell activation by flow cytometry with or without anti-CD3/CD28 Ab activation. (A) Percentage of live PMBCs (Zombie negative) and activated CD3<sup>+</sup> T cells (CD69 positive) were detected in RCA-treated or control group without anti-CD3/CD28 Ab treatment. (B) Upon activation by anti-CD3/CD28 Ab, percentage of live PMBCs (Zombie negative) and CD69, IL-2, IFN- $\gamma$  positive CD3<sup>+</sup> T cells were detected in RCA-treated or control group. Data were shown as mean  $\pm$  SEM; \* $P < 0.05$ , \*\* $P < 0.01$ , \*\*\* $P < 0.001$ .

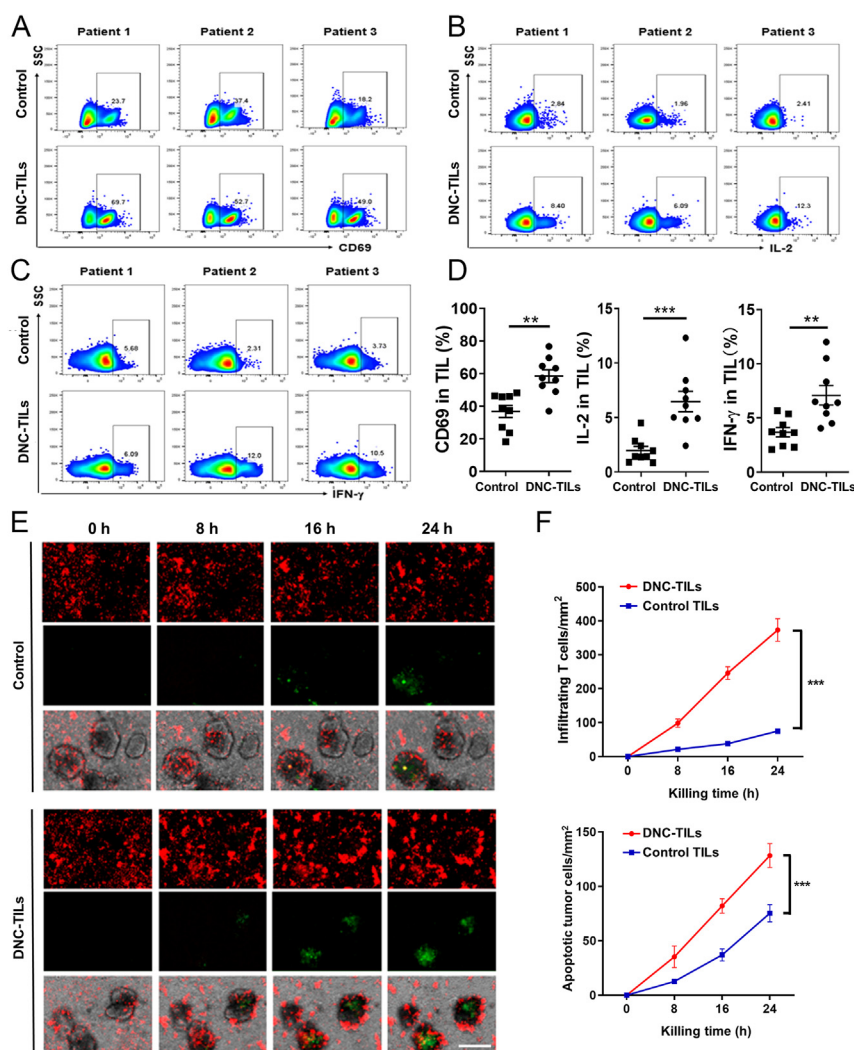


**Figure 6** Coating with DNA network promoted activation and tumor killing activities of TILs in *ex-vivo* human liver cancer organoid killing model. After *ex vivo* expansion, human TILs isolated from primary liver cancer patients were pretreated with RCA reactions for 1 h, to form DNA network-coated TILs (DNC-TILs), and then co-cultured with autologous tumor organoids at an *E:T* ratio of 10:1 for organoid killing assay at indicated time points. (A–D) After 6 h co-culture, (A) CD69 expression as well as (B) IL-2 and (C) IFN- $\gamma$  production in TILs for RCA or control-treated group were analyzed by flow cytometry. (D) The percentage of CD69, IL-2, IFN- $\gamma$  positive TILs were calculated and data were shown as mean  $\pm$  SEM;  $n = 9$ ; \* $P < 0.05$ , \*\* $P < 0.01$ , \*\*\* $P < 0.001$ . (E–F) TILs prestained with CellTrace Far Red (red) were co-cultured with autologous tumor organoids, in the presence of cell apoptosis probe, cell apoptosis (green) was visualized at indicated time points of killing (0, 8, 16, and 24 h). (E) Representative immunofluorescence microphotography images were shown and (F) the number of infiltrating T cells as well as apoptotic tumor cells in the organoids were quantified using Imaris software. Scale bar: 200  $\mu$ m.

reactive oxygen species (ROS). As shown in Fig. 4B–F, the cell viability of DNC–Cells and DNC–Cell clusters was much higher than that in native cells, in response to harmful stimuli like UV exposure, high speed centrifugation, as well as unfavorable culture conditions, demonstrating the protective role of DNA network coating on the cell surface. Moreover, cell viability was significantly enhanced in DNC–Cell cluster *vs.* DNC–Cell group, suggesting that upon DNA network coating, cell clusters were more resistant to external stimuli than dispersing cells.

### 3.7. Selective coating with DNA network promoted T cell activation in human PBMCs without affecting cell viability

To further access the effect of DNA network on primary lymphocytes, human PBMCs were pretreated with RCA reactions or

control vehicles at indicated time points, followed with or without agonistic anti-CD3/CD28 Ab treatment, and then detected for cell viability and T cell activation by flow cytometry. Data show that the cell viability were comparable in control and RCA-treated PBMC within 2 h treatment, while expression of CD69, the activation marker of T cells, were dramatically enhanced in RCA-treated *vs.* control group, with or without anti-CD3/CD28 Ab activation (Fig. 5A and B). Moreover, upon activation by anti-CD3/CD28 Ab, production of IL-2 and IFN- $\gamma$  in T cells were also enhanced in RCA-treated *vs.* control group (Fig. 5B). These data together indicated that coating with DNA network promoted T cell activation in human PBMCs without affecting cell viability. When compared T cell viability and activity at indicated time points for RCA reaction, the optimal reaction time was 1 h, and therefore this reaction time was applied in the following experiments.

### 3.8. Coating with DNA network promoted activation and tumor killing activities of TILs in an *ex vivo* human liver cancer organoid killing model

Since T cell activation is the prerequisite of efficient tumor killing, next, we used an *ex vivo* tumor organoid killing model to evaluate the effect of DNA network on TIL. After *ex vivo* expansion, human TILs isolated from primary liver cancer patients were pretreated with RCA reactions for 1h, to form DNA network-coated TILs (DNC-TILs), and then co-cultured with their autologous tumor organoids at an *E:T* ratio of 10:1 for organoid killing assay at indicated time points. Then, the activity and killing efficiency of TILs were analyzed by flow cytometry or immunofluorescent staining, respectively. Flow cytometry data show that after 6 h co-culture with organoids, DNC-TILs displayed more CD69 expression as well as IL-2 and IFN- $\gamma$  production, when compared with that in control-treated group (Fig. 6A–D). Moreover, immunofluorescence microphotography data showed that at indicated time points of killing (0, 8, 16, and 24 h), more DNC-TILs (red) infiltrated into tumor organoids, and more apoptotic tumor cells (green) were detected within organoids (Fig. 6E and F). These data indicate that coating with DNA network promoted activation and tumor killing activities of TILs.

## 4. Conclusion

T cells are the most widely used lymphocytes in ACT. However, primary T cells isolated from human body must undergo activation and expansion before usage, while the *in vitro* process of lymphocyte preservation during transfer, manipulation and storage may compromise the cell viability and biological activities. Therefore, a high-efficient cell protection strategy is necessary to enhance therapeutic efficacy of ACT.

In the present study, we developed a novel T cell-protective strategy by constructing a flexible DNA network on T-cell surface. Although several cell protection strategies have been reported previously, their application in ACT are still limited. To date, the most common cell-coating strategy was based on the deposition of polyelectrolytes or minerals or metal ion complexation on cell membrane<sup>11</sup>. However, these materials with strong stiffness and poor deformability often form a tight and hard shell on cell surface, which may compromise the binding of T-cell surface receptors to their ligands expressed on other cells (like antigen-presenting cells or tumor cells)<sup>12,18,20,24–26</sup>, and therefore suppressing T-cell activation and killing efficiency. Moreover, if not treated with proper concentration or time, the deposited monomers or degraded polymers<sup>21–23</sup> or metal ion complexation display varying degrees of toxicity, losing their cytoprotective property. In contrast, DNA materials, especially DNA network, display great advantages as an ideal cell coating material, for their excellent performance on biocompatibility, stability, accessibility, as well as precise programmability and functionalization<sup>9,27–29,32,33</sup>. These advantages make the DNA materials fit to living cell encapsulation and the following *in vivo* applications.

Previous DNA-based strategies usually need a complex multi-step cross-linking progress<sup>27</sup>. While in the present study, we established a novel DNA coating strategy based on *in situ* RCA reaction. Using a trivalent tetrahedral DNA nanostructure as a rigid scaffold, this RCA reaction can occur on cell membrane and produce many flexible long single strand DNAs, and thereby form a flexible DNA network as a protective surface shell. This *in situ*

RCA reaction only takes one-step reaction, and thus is much simpler and time-saving than other cytoprotective methods.

Furthermore, since T cells are the most important effector cells in ACT, we added a T-cell specific aptamer in the T cell-targeted trivalent tetrahedral DNA nanostructure, to make sure the *in situ* RCA reaction was performed specifically on T-cell surface. The efficiency and specificity of this DNA-based selective coating for T cells was confirmed in mixed cells containing both T cells (Jurkat) and tumor cells (MCF-7) as well as in human PBMCs. So far, selective coating is lacking in most of the current cell-protection strategies using polyelectrolytes<sup>19</sup>, minerals<sup>6</sup>, nanoparticles<sup>7</sup> and phospholipid modified DNA oligonucleotides<sup>9,27</sup>. Hence, the prerequisite step before living cell encapsulation is the isolation of target cells. During this process, some sensitive and fragile cells may be harmed by unfavorable stimuli, and thereby reducing the acquisition efficiency and viability of target cells. Our study demonstrated that Jurkat cells coated with the flexible DNA network were highly resistant to external stimuli like UV exposure, relative centrifugal force, pH, osmotic pressure and ROS, indicating that this high-efficient and selective cytoprotective method is very suitable to be applied in ACT. To be noted, along with the RCA reaction time, the DNA network on T-cell surface may entangled with each other, leading to T cell aggregation and formation of T-cell cluster with different sizes. Based on the literature, clustered cells displayed more anti-apoptosis ability as well as highly mobility than single cell suspension<sup>46,47</sup>. In the organoid killing model, TILs also formed small clusters to attack autologous tumor organoids. Using primary PBMCs or human liver cancer organoid killing model, we demonstrated that DNC-clusters were more efficient than DNC-cells in activation and tumor killing, and the optimal reaction time of RCA was around 1 h, indicating that the size of T cell clusters may be important for biomedical application in ACT.

Overall, we successfully established a novel DNA-based selective coating method for T cells, which can enhance their resistance to external stimuli and promote T cell activation as well as tumor killing efficiency. This selective coating strategy may also be applied to other cell types, by changing the cell-specific aptamer in the DNA nanostructure, and may expected to protect T cell *in vivo* too, for example, cell membrane damage caused by physical stresses generated from cell injection and intravascular circulation<sup>48</sup>, immunosuppression due to acidic tumor microenvironment<sup>49</sup>, therefore displays a great potential for application in ACT.

## Acknowledgements

This work was supported by the National Natural Science Foundation of China, China (82072087, 31670880 and 31970893); Guangdong Natural Science Fund for Distinguished Young Scholars, China (2017A030306016 and 2016A030306004); Fundamental Research Funds for the Central Universities, China (19ykzd39).

## Author contributions

Ziyan Zhang, Qiaojuan Liu and Jizhou Tan designed and performed the experiments, interpreted the data, and wrote the manuscript. Qiaojuan Liu, Ziyan Zhang and Xiaoxia Zhan did the study of PBMCs. Jizhou Tan and Ting Liu did the study of liver cancer organoid killing model. Yuting Wang participated part of the experiments. Gen Lu revised the manuscript. Minhao Wu and Yuanqing Zhang conceived the study, interpreted the data, wrote

and revised the manuscript. All of the authors have read and approved the final manuscript.

### Conflicts of interest

The authors have no conflicts of interest to declare.

### Appendix A. Supporting information

Supporting data to this article can be found online at <https://doi.org/10.1016/j.apsb.2021.04.002>.

### References

- Waldman AD, Fritz JM, Lenardo MJ. A guide to cancer immunotherapy: from T cell basic science to clinical practice. *Nat Rev Immunol* 2020;**20**:651–68.
- Zhao ZJ, Chen Y, Francisco NM, Zhang YQ, Wu MH. The application of CAR-T cell therapy in hematological malignancies: advantages and challenges. *Acta Pharm Sin B* 2018;**8**:539–51.
- Rohaam MW, Wilgenhof S, Haanen J. Adoptive cellular therapies: the current landscape. *Virchows Arch* 2019;**474**:449–61.
- Guedan S, Ruella M, June CH. Emerging cellular therapies for cancer. *Annu Rev Immunol* 2019;**37**:145–71.
- Lee J, Choi J, Park JH, Kim MH, Hong D, Cho H, et al. Cytoprotective silica coating of individual mammalian cells through bioinspired silicification. *Angew Chem Int Ed Engl* 2014;**53**:8056–9.
- Youn W, Ko EH, Kim MH, Park M, Hong D, Seisenbaeva GA, et al. Cytoprotective encapsulation of individual Jurkat T cells within durable TiO<sub>2</sub> shells for T-cell therapy. *Angew Chem Int Ed Engl* 2017;**56**:10702–6.
- Zhu W, Guo JM, Amini S, Ju Y, Agola JO, Zimpel A, et al. Supra-Cells: living mammalian cells protected within functional modular nanoparticle-based exoskeletons. *Adv Mater* 2019;**31**:1900545.
- Lee J, Cho H, Choi J, Kim D, Hong D, Park JH, et al. Chemical sporulation and germination: cytoprotective nanocoating of individual mammalian cells with a degradable tannic acid-Fe<sup>III</sup> complex. *Nano-scale* 2015;**7**:18918–22.
- Shi P, Zhao N, Coyne J, Wang Y. DNA-templated synthesis of biomimetic cell wall for nanoencapsulation and protection of mammalian cells. *Nat Commun* 2019;**10**:2223.
- Park JH, Hong D, Lee J, Choi IS. Cell-in-shell hybrids: chemical nanoencapsulation of individual cells. *Acc Chem Res* 2016;**49**:792–800.
- Hasturk O, Kaplan DL. Cell armor for protection against environmental stress: advances, challenges and applications in micro- and nanoencapsulation of mammalian cells. *Acta Biomater* 2019;**95**:3–31.
- Yang JM, Li JC, Li XM, Wang XL, Yang YJ, Kawazoe N, et al. Nanoencapsulation of individual mammalian cells with cytoprotective polymer shell. *Biomaterials* 2017;**133**:253–62.
- Matsuzawa A, Matsusaki M, Akashi M. Effectiveness of nanometer-sized extracellular matrix layer-by-layer assembled films for a cell membrane coating protecting cells from physical stress. *Langmuir* 2013;**29**:7362–8.
- Yang JM, Yang YJ, Kawazoe N, Chen G. Encapsulation of individual living cells with enzyme responsive polymer nanoshell. *Biomaterials* 2019;**197**:317–26.
- Levine BL, Miskin J, Wonnacott K, Keir C. Global manufacturing of CAR T cell therapy. *Mol Ther Methods Clin Dev* 2017;**4**:92–101.
- Tyagarajan S, Spencer T, Smith J. Optimizing CAR-T cell manufacturing processes during pivotal clinical trials. *Mol Ther Methods Clin Dev* 2020;**16**:136–44.
- Lee JK, Choi IS, Oh TI, Lee E. Cell-surface engineering for advanced cell therapy. *Chem Eur J* 2018;**24**:15725–43.
- Hwang J, Choi D, Choi M, Seo Y, Son J, Hong J, et al. Synthesis and characterization of functional nanofilm-coated live immune cells. *ACS Appl Mater Interfaces* 2018;**10**:17685–92.
- Pandey S, Afrin F, Tripathi RP, Gangenahalli G. Human T-cell line (Jurkat cell) encapsulation by nano-organized polyelectrolytes and their response assessment *in vitro* and *in vivo*. *J Nanopart Res* 2013;**15**:1793.
- Park T, Kim JY, Cho H, Moon HC, Kim BJ, Park JH, et al. Artificial spores: immunoprotective nanocoating of red blood cells with supramolecular ferric ion-tannic acid complex. *Polymers* 2017;**9**:140.
- Fischer D, Li YX, Ahlemeyer B, Krieglstein J, Kissel T. *In vitro* cytotoxicity testing of polycations: influence of polymer structure on cell viability and hemolysis. *Biomaterials* 2003;**24**:1121–31.
- Hong S, Leroueil PR, Janus EK, Peters JL, Kober MM, Islam MT, et al. Interaction of polycationic polymers with supported lipid bilayers and cells: nanoscale hole formation and enhanced membrane permeability. *Bioconjugate Chem* 2006;**17**:728–34.
- Jeong H, Hwang J, Lee H, Hammond PT, Choi J, Hong J. *In vitro* blood cell viability profiling of polymers used in molecular assembly. *Sci Rep* 2017;**7**:9481.
- Mansouri S, Merhi Y, Winnik FM, Tabrizian M. Investigation of layer-by-layer assembly of polyelectrolytes on fully functional human red blood cells in suspension for attenuated immune response. *Bio-macromolecules* 2011;**12**:585–92.
- Kim JY, Lee H, Park T, Park J, Kim MH, Cho H, et al. Artificial spores: cytocompatible coating of living cells with plant-derived pyrogallol. *Chem Asian J* 2016;**11**:3183–7.
- Wang B, Wang GC, Zhao BJ, Chen JJ, Zhang XY, Tang RK. Antigenically shielded universal red blood cells by polydopamine-based cell surface engineering. *Chem Sci* 2014;**5**:3463–8.
- Gao T, Chen TS, Feng C, He X, Mu CL, Anzai JJ, et al. Design and fabrication of flexible DNA polymer cocoons to encapsulate live cells. *Nat Commun* 2019;**10**:2946.
- Zhang YZ, Tu J, Wang DQ, Zhu HT, Maity SK, Qu XM, et al. Programmable and multifunctional DNA-based materials for biomedical applications. *Adv Mater* 2018;**30**:1703658.
- Ebrahimi SB, Samanta D, Mirkin CA. DNA-based nanostructures for live-cell analysis. *J Am Chem Soc* 2020;**142**:11343–56.
- Gao H, Zhang KX, Teng XC, Li JH. Rolling circle amplification for single cell analysis and *in situ* sequencing. *TrAC Trends Anal Chem* 2019;**121**:115700.
- Li J, Lin L, Yu JT, Zhai SY, Liu GY, Tian LL. Fabrication and biomedical applications of “polymer-like” nucleic acids enzymatically produced by rolling circle amplification. *ACS Appl Bio Mater* 2019;**2**:4106–20.
- Tang JP, Yao C, Gu Z, Jung S, Luo D, Yang DY. Super-soft and super-elastic DNA robot with magnetically driven navigational locomotion for cell delivery in confined space. *Angew Chem Int Ed Engl* 2020;**59**:2490–5.
- Yao C, Tang H, Wu WJ, Tang JP, Guo WW, Luo D, et al. Double rolling circle amplification generates physically cross-linked DNA network for stem cell fishing. *J Am Chem Soc* 2020;**142**:3422–9.
- Lin MH, Wang JJ, Zhou GB, Wang JB, Wu N, Lu JX, et al. Programmable engineering of a biosensing interface with tetrahedral DNA nanostructures for ultrasensitive DNA detection. *Angew Chem Int Ed Engl* 2015;**54**:2151–5.
- Liu Q, Ge ZL, Mao XH, Zhou GB, Zuo XL, Shen JW, et al. Valency-controlled framework nucleic acid signal amplifiers. *Angew Chem Int Ed Engl* 2018;**57**:7131–5.
- Han X, Xu X, Wu ZH, Wu ZH, Qi XL. Synchronous conjugation of i-motif DNA and therapeutic siRNA on the vertexes of tetrahedral DNA nanocages for efficient gene silence. *Acta Pharm Sin B* 2021. Available from: <https://doi.org/10.1016/j.apsb.2021.02.009>.
- Li J, Xun KY, Pei K, Liu XJ, Peng XY, Du YL, et al. Cell-membrane-anchored DNA nanoplatfor for programming cellular interactions. *J Am Chem Soc* 2019;**141**:18013–20.

38. Li M, Ding HM, Lin MH, Yin FF, Song L, Mao XH, et al. DNA framework-programmed cell capture *via* topology-engineered receptor-ligand interactions. *J Am Chem Soc* 2019;**141**:18910–5.
39. Peng P, Wang QW, Du Y, Wang HH, Shi LL, Li T. Extracellular ion-responsive logic sensors utilizing DNA dimeric nanoassemblies on cell surface and application to boosting AS1411 Internalization. *Anal Chem* 2020;**92**:9273–80.
40. Qin WW, Chen L, Wang ZR, Li Q, Fan CH, Wu MH, et al. Bioinspired DNA nanointerface with anisotropic aptamers for accurate capture of circulating tumor cells. *Adv Sci* 2020;**7**:2000647.
41. Yin FF, Li M, Mao XH, Li F, Xiang XL, Li Q, et al. DNA framework-based topological cell sorters. *Angew Chem Int Ed Engl* 2020;**59**:10406–10.
42. Zhuang JL, Tan JZ, Wu CL, Zhang J, Liu T, Fan C, et al. Extracellular vesicles engineered with valency-controlled DNA nanostructures deliver CRISPR/Cas9 system for gene therapy. *Nucleic Acids Res* 2020;**48**:8870–82.
43. Broutier L, Mastrogianni G, Versteegen MM, Francies HE, Gavarró LM, Bradshaw CR, et al. Human primary liver cancer-derived organoid cultures for disease modeling and drug screening. *Nat Med* 2017;**23**:1424–35.
44. Yang Y, Sun XQ, Xu J, Cui C, Safari Yazd H, Pan XS, et al. Circular bispecific aptamer-mediated artificial intercellular recognition for targeted T cell immunotherapy. *ACS Nano* 2020;**14**:9562–71.
45. Liu XW, Yan H, Liu Y, Chang Y. Targeted cell–cell interactions by DNA nanoscaffold-templated multivalent bispecific aptamers. *Small* 2011;**7**:1673–82.
46. Aceto N, Bardia A, Miyamoto DT, Donaldson MC, Wittner BS, Spencer JA, et al. Circulating tumor cell clusters are oligoclonal precursors of breast cancer metastasis. *Cell* 2014;**158**:1110–22.
47. Hou JM, Krebs M, Ward T, Sloane R, Priest L, Hughes A, et al. Circulating tumor cells as a window on metastasis biology in lung cancer. *Am J Pathol* 2011;**178**:989–96.
48. Choi D, Lee H, Kim HB, Yang M, Heo J, Won Y, et al. Cytoprotective self-assembled RGD peptide nanofilms for surface modification of viable mesenchymal stem cells. *Chem Mater* 2017;**29**:2055–65.
49. Leone RD, Powell JD. Metabolism of immune cells in cancer. *Nat Rev Cancer* 2020;**20**:516–31.